Helicopter Air Resonance Modeling and Suppression Using Active Control

M. D. Takahashi* and P. P. Friedmann†
University of California, Los Angeles, Los Angeles, California 90024

A coupled rotor/fuselage helicopter analysis with the important effects of blade torsional flexibility, unsteady aerodynamics, and forward flight is presented. Using this mathematical model, a nominal configuration is selected with an air resonance instability throughout most of its flight envelope. A multivariable compensator is then designed using two swashplate inputs and a single-body roll rate measurement. The controller design is based on the linear quadratic Gaussian technique and the loop transfer recovery method. The controller is shown to suppress the air resonance instability throughout a wide range of helicopter loading conditions and forward flight speeds.

Nomenclature‡

AR = horizontal tail aspect ratio
a = rotor blade lift curve slope
a_T = horizontal tail lift curve slope
b = blade semichord
C_{d0} = blade drag coefficient
C_{d0T} = horizontal tail drag coefficient
e = hinge offset
f = fuselage drag area, $\bar{f}/2\bar{b}\bar{R}$
I_B = blade flap inertia about the hinge offset
I_{Cxx}, I_{Cyy} = fuselage roll and pitch inertias
J_x = blade pitch inertia
J_y, J_z = integral of the blade flap and lead-lag bending inertias
K_x, K_y, K_z = flap, lag, and torsion spring constants, respectively
l = blade length
$\bar{M}_B$ = dimensional blade mass
M_F = fuselage mass
N_b = number of blades
$\bar{R}$ = dimensional rotor radius
R_c = elastic coupling coefficient
R_x, R_y, R_z = translational degrees of freedom of the fuselage
S_T = horizontal tail area
V = forward flight speed
w_s, w_o = state and observation noise processes
x_A = blade aerodynamic center offset from the blade elastic axis
x_b, y_b, z_b = blade center-of-mass position from the hinge offset
X_{MC}, Z_{MC} = position of the fuselage center-of-mass
X_{MH}, Z_{MH} = position of the rotor hub center
X_{MT}, Z_{MT} = position of the horizontal tail aerodynamic center
α_R = rotor trim pitch angle
β_p = blade precone angle
γ = lock number
θ_{pk} = pitch of the kth blade
θ_x, θ_y = roll and pitch degrees of freedom
$\theta_0, \theta_{1s}, \theta_{1c}$ = collective, sine, and cosine inputs
μ = advance ratio, $V\cos(\alpha_R)/\bar{R}\bar{\Omega}$
σ = solidity ratio, $2N_b/\pi$
$\bar{\sigma}[\,]$ = maximum singular value
ψ_k = kth blade azimuth angle
$\bar{\Omega}$ = dimensional rotor rate
$\Omega_{F1}, \omega_{L1}, \omega_{T1}$ = rotating first flap, lag, and torsional blade frequencies
$[\dot{}]$ = nondimensional time derivative, $d[\,]/d\psi$

Introduction

THE need to reduce the mechanical complexity and weight of the rotor hub on helicopters has generated considerable interest in hingeless and bearingless rotors. Although these new rotor configurations are simple and lightweight, they can introduce other undesirable dynamic problems. One important problem that can arise in soft-in-plane rotor systems is "air resonance," and is a condition where the blade lead-lag motions strongly interact with the fuselage pitch or roll motion in flight.[1,2] This aeromechanical phenomenon produces large fuselage oscillations and is clearly undesirable when unstable or weakly stable. The approach to suppressing ground resonance in articulated rotor systems has been through lead-lag dampers for each rotor blade. This approach can also be applied to air resonance of hingeless rotors systems, but this solution tends to destroy the mechanical simplicity and aerodynamic cleanliness inherent in hingeless and bearingless rotors. Another possible means of stabilizing or augmenting stability of air resonance is through an active controller operating with a conventional swashplate.

Research in the active control of air and ground resonance is limited to a few references.[3-5] The helicopter models used in these studies were limited since important effects such as torsional flexibility of the rotor blades, forward flight, and unsteady aerodynamics were all neglected. Furthermore, the studies dealing with the active control of air resonance did not adequately demonstrate the ability of the control schemes to operate throughout the wide range of operating conditions that can normally be encountered. In order to remedy the situation just described, a coupled rotor/fuselage model, in which the important effects of forward flight, unsteady aerodynamics, and blade torsional flexibility are considered, is used to demonstrate that simple active controllers can be designed to suppress air resonance throughout a wide range of operating conditions.

Received Sept. 14, 1989; revision received Sept. 17, 1990; accepted for publication Oct. 2, 1990.

*Doctoral Candidate; currently, Research Engineer, U.S. Army Aviation Research and Technology Activity, Mail Stop 211-2, Moffett Field, CA 94035.

†Professor, Mechanical, Aerospace, and Nuclear Engineering Department. Fellow AIAA.

‡Variables with an overbar are dimensional. Unless otherwise stated, variables without an overbar are nondimensionalized by the blade mass $\bar{M}_B$, rotor radius $\bar{R}$, and the rotor speed $\bar{\Omega}$.

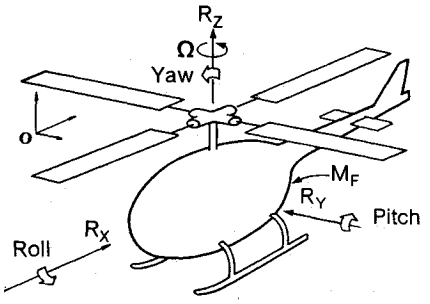

Fig. 1 Rotor/fuselage configuration.

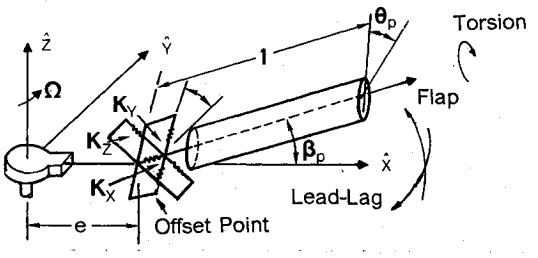

Fig. 2 Offset-hinged, spring-restrained, rigid-rotor blade model.

Mathematical Model

The mathematical model of the rotor/fuselage system that is used in this paper is the model documented in Refs. 6 and 8. For more details on the model, and the helicopter configuration that is described in the next section, the reader is referred to Refs. 6 and 8. The fuselage is represented as a rigid body with five degrees of freedom, where three of these are linear translations and two are angular positions of pitch and roll (Fig. 1). Yaw is ignored since its effect in the air resonance problem is known to be small. An offset-hinged, spring-restrained, rigid blade model is used to represent a hingeless rotor blade as depicted in Fig. 2. This assumption simplifies the equations of motion, while retaining the essential features of the air resonance problem. In this model, the blade elasticity is concentrated at a single point called the hinge-offset point, and torsional springs are used to represent this flexibility. The dynamic behavior of the rotor blade is represented by three degrees of freedom for each blade, which are flap, lag, and torsion motions. The aerodynamic loads of the rotor blades are calculated using a quasisteady two-dimensional potential flow strip theory. Compressibility and dynamic stall effects are neglected, although they could be important at high advance ratios. Unsteady aerodynamic effects, which are created by the time-dependent wake shed by the airfoil as it undergoes arbitrary time-dependent motion, are accounted for by using a dynamic inflow model. This model is described by a three-state linear model forced by perturbations in the aerodynamic thrust, roll moment, and pitch moment at the rotor hub. The three states of these equations describe the behavior of perturbations in the induced inflow through the rotor plane. The model coefficients used in this paper are those of Ref. 7.

The equations of motion of the coupled rotor/fuselage system are complex and contain geometric nonlinear terms due to moderate blade deflections in the aerodynamic, inertial, and structural forces. For this reason, the equations were derived and analytically linearized about the helicopter trim using a symbolic manipulation program. An ordering scheme was applied to the problem to further simplify the equation derivation. There are five fuselage equations, of which three enforce the fuselage translational equilibrium and two enforce the roll and pitch equilibrium. For each blade, there are three equations, which are associated with the flap, lag, and torsion motions of the blade. In addition, there are three aerodynamic forces and moments at the hub, whose perturbations about the vehicle trim drive the three-state dynamic inflow model.

The active control inputs to suppress the air resonance instability are those of a swashplate. The pitch of the kth rotor blade is given by the expression

$$\theta_{pk} = (\theta_0 + \Delta\theta_0) + (\theta_{1c} + \Delta\theta_{1c})\cos(\psi_k) + (\theta_{1s} + \Delta\theta_{1s})\sin(\psi_k) \quad (1)$$

The Δ terms are small and these represent the active control inputs, while those without Δ are the inputs necessary to trim the vehicle.

The stability of the system is determined through the linearization of the equations of motion about a blade equilibrium solution and the helicopter trim solution. The helicopter trim and equilibrium solution are extracted simultaneously using harmonic balance for a straight-and-level flight condition. After linearization, a multi-blade coordinate transformation is applied, which transforms the set of rotating blade degrees of freedom to a set of hub-fixed nonrotating coordinates. This transformation is introduced in order to take advantage of the favorable properties of the nonrotating coordinate representation. The untransformed system has periodic coefficients with a fundamental frequency of 1/rev; however, the transformed system has coefficients with a higher fundamental frequency. These higher-frequency periodic terms have a reduced influence on the behavior of the system and can be ignored in some analyses at low advance ratios. In hover, the untransformed system has periodic coefficients with a frequency of 1/rev, but the transformed system has constant coefficients. Two other properties of the model in hover are that the collective modes decouple from the sine and cosine modes of the system, and the differential modes become uncontrollable. Thus, in hover, depending on what outputs and inputs are selected, the model may have uncontrollable and unobservable modes.

Once the transformation is carried out, the system is rewritten in first-order form:

$$\dot{x} = A(\psi)x + B(\psi)u \quad (2)$$

The fundamental frequency of the coefficient matrices depends on the number of rotor blades. For an odd number of blades, the fundamental frequency is N_b per revolution, whereas for an even number of blades the fundamental frequency is $N_b/2$ per revolution. The system is constant coefficient in hover and becomes more periodic as the flight speed is increased. Stability can be determined either by using an eigen-

Table 1 Data of the nominal configuration

Characteristic dimensions

Blade mass	= 52 kg
Rotor radius	= 4.9 m
Rotor rate	= 425 rpm

Rotor data

l	= 0.85	e	= 0.15	ω_{F1}	= 1.15 at zero pitch
x_b	= 0.36	γ	= 5.0	ω_{L1}	= 0.620
I_b	= 0.18	C_{d0}	= 0.01	ω_{T1}	= 3.00
J_x	= 0.00015	a	= 5.90	0.5% damping	
J_y	= 0	x_A	= 0	σ	= 0.07
J_z	= 0.00015	y_b	= 0	R_c	= 1.0
β_p	= 0	b	= 0.02749	N_b	= 4.0
μ_{cruise}	= 0.3				

Fuselage data

M_F	= 32	f	= 0.60
I_{Cxx}	= 1.0	Z_{MH}	= 0.2667
I_{Cyy}	= 4.0	Z_{MC}	= 0.0333

Horizontal tail data

X_{MT}	= 1.0	a_T	= 5.0
S_T	= 0.04	C_{d0T}	= 0.007
AR	= 5.5		

value analysis or by using Floquet theory for the periodic problem in forward flight. An approximate stability analysis in forward flight is also possible by performing an eigenvalue analysis on the constant-coefficient portion of the system matrices of Eq. (2).

The mathematical model was tested by comparing results to other analytical and experimental results. The correlation with these results was good and verified that the effects of torsion, unsteady aerodynamics, and forward flight were accurately represented in the model.

Helicopter Configuration

The helicopter configuration used in this paper is the same as the "nominal configuration" in Ref. 8, and the data for the configuration are shown in Table 1. The parameters are selected to make the nominal configuration a four-bladed light helicopter with an unstable air resonance mode. The five body degrees of freedom and the twelve rotor degrees of freedom (three degrees of freedom for each blade) produce 34 position and rate states. The dynamic inflow model augments the system with three more states giving a total system order of 37. Figure 3 shows the eigenvalues in the s plane of the modes of the nominal configuration at an advance ratio of 0.3. The lead-lag regressing mode is associated with the air resonance instability and is mildly unstable in this flight condition. It is with the body roll mode that the lead-lag regressing mode interacts. Thus, for this particular configuration, the dominant body motion of the instability is the rolling motion of the fuselage.

The parameter variations considered in this paper are limited to those that change during the normal operation of the helicopter. Thus, the significant parameters are the advance ratio μ, fuselage mass M_F, fuselage inertias I_{Cxx}, I_{Cyy}, and the fuselage center of gravity position X_{MC}, Z_{MC}. Checking the stability for every combination of these parameters would require an excessive amount of labor. Since an increase in the fuselage mass also results in an increase in the fuselage inertias, there is no need to consider cases that combine increases in fuselage mass with decreases in inertias. A simpler approach is to use approximate expressions that relate the fuselage mass to the other pertinent parameters. Thus, I_{Cxx}, I_{Cyy}, and Z_{MC} all become functions of M_F. The precise expressions for these relationships can be found in Ref. 6. The parameter X_{MC} is ignored since it was found that expected changes in this parameter insignificantly affected the air resonance instability. The remaining parameters can greatly affect the air resonance instability, since they influence the body frequencies.

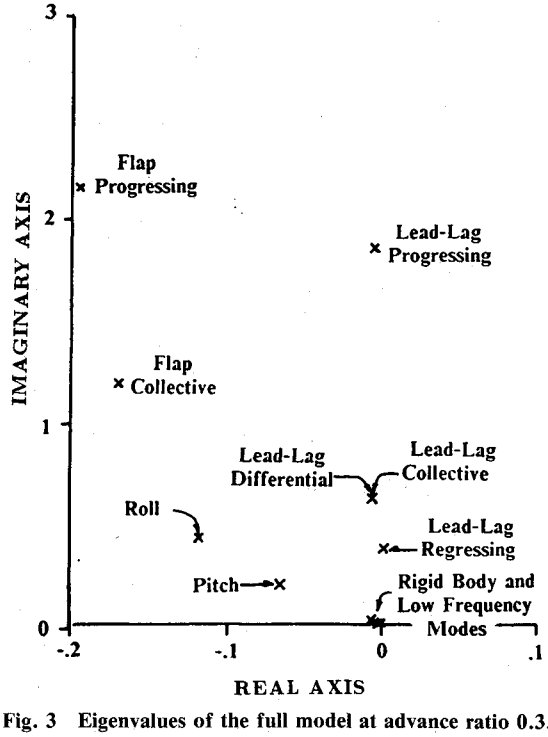

Fig. 3 Eigenvalues of the full model at advance ratio 0.3.

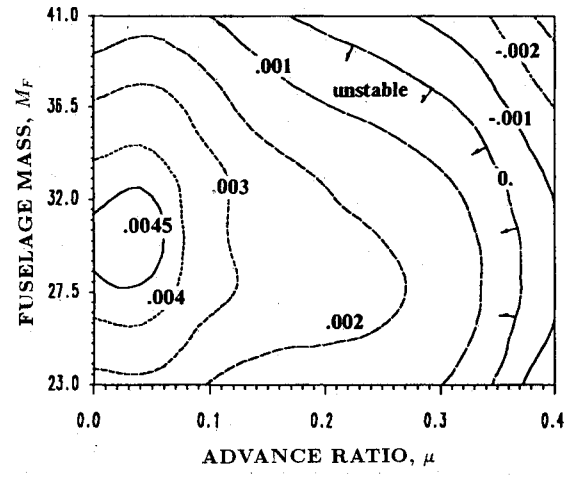

Fig. 4 Open-loop nondimensional real part of the lead-lag regressing eigenvalue at various fuselage weights and advance ratios.

The real part of the open-loop lead-lag regressing eigenvalue of the helicopter configuration throughout its flight regime is presented in Fig. 4. The horizontal axis is the advance ratio, whereas the vertical axis is the fuselage mass nondimensionalized by the blade mass of 52 kg. A nondimensional fuselage mass of 32 plus four blades corresponds to the nominal total mass of 1872 kg. The figure indicates the system experiences an air resonance instability throughout most of the flight regime. Marginal stability exists at an advance ratio greater than 0.35 and the operating point where the air resonance mode is least stable is at $M_F = 30$ and in the vicinity of hover.

Additional insight on this helicopter configuration was gained in Ref. 8, where preliminary studies were conducted at the nominal weight to assess the importance of various modeling effects. In these studies, full state feedback from the linear deterministic optimal regulator problem was used and the relevant results that will be used throughout this paper follow:

1) The torsional degree of freedom and unsteady aerodynamics are important effects in an air resonance controller design model. Significant errors can arise in the closed-loop damping if these effects are ignored.

2) The collective pitch input is not important in controlling the air resonance instability in forward flight up to advance ratios of 0.4.

3) The periodic coefficients of the linearized model have a small effect on the open- and closed-loop damping of the air resonance mode for advance ratios up to 0.4. Thus, the constant-coefficient approximation of the model should be sufficient for the initial control design.

Item 3 is particularly relevant in that it allows the design and stability analysis to be done using a constant-coefficient model (i.e., the constant portion of A and B). However, because of the inherent periodic nature of the system a final check of the periodic stability must be done.

Compensator Design Method

The controller to suppress the air resonance instability of the helicopter configuration is based on the optimal state estimator in conjunction with optimal feedback gains [linear quadratic Gaussian (LQG)]. A constant-coefficient model is assumed, since the results of the preliminary control studies of Ref. 8 indicated a periodic model was unnecessary. The compensator has the well-known form

$$K(s) = K_c(sI - A + BK_c + K_fC)^{-1}K_f \qquad (3)$$

where the filter gains K_f result from the solution of a Riccati equation, which is a function of the system and the covariances of the state noise w_s and the observation noise w_o. The feedback gains K_c result from the solution of a Riccati equation, which is a function of the system and the state weight matrix Q and the control weight matrix R.

The approach just outlined is a powerful approach to feedback design; however, if the design model differs from the actual plant to be controlled, poor performance and even instability can occur. The possibility of a controller lacking "robustness" is not surprising, since no provision is made to account for uncertainty in the design process. In all applications, the design model and the actual plant to be controlled will have unavoidable differences due to the limitations associated with formulating models of physical systems. Our objective in this paper is to design a low-order controller at an operating condition and require it to function adequately at the off-design conditions. Thus, the differences between the design model and the actual plant to be controlled will be exacerbated. An additional drawback of the design method just described is that there are many possible choices of design variables in the covariance, state weight, and input weight matrices. This selection process is difficult without the use of important concepts (e.g., bandwidth) that have proved so useful in single-input single-output (SISO) time-invariant linear control design.[9] To overcome these difficulties, the multivariable frequency-domain design methods of Refs. 10 and 11 are used. This will allow interpretation of the design process using frequency-domain concepts and account for the possibility of high-frequency modeling error.

The introduction of uncertainty into the design method stated above comes about through the representation of model error. One representation of this error is in the form of an unstructured multiplicative uncertainty at the model output.

$$G_{\text{off}}(s) = [I+L(s)]G(s) \tag{4}$$

Other unstructured uncertainty models are available depending on the type of modeling errors one encounters, but for the objectives of this paper Eq. (4) is quite sufficient. What are of particular interest are the singular values of the uncertainty matrix L, in particular, the maximum singular value, which defines the error function

$$l_m(\omega) = \bar{\sigma}[L(j\omega)] \tag{5}$$

The error function $l_m(\omega)$ characterizes the magnitude of the modeling error at all frequencies. A stability condition on the closed-loop system using this error function is

$$\bar{\sigma}[T(j\omega)] = \bar{\sigma}[G(s)K(s)(I+G(s)K(s))^{-1}] < 1/l_m(\omega) \tag{6}$$

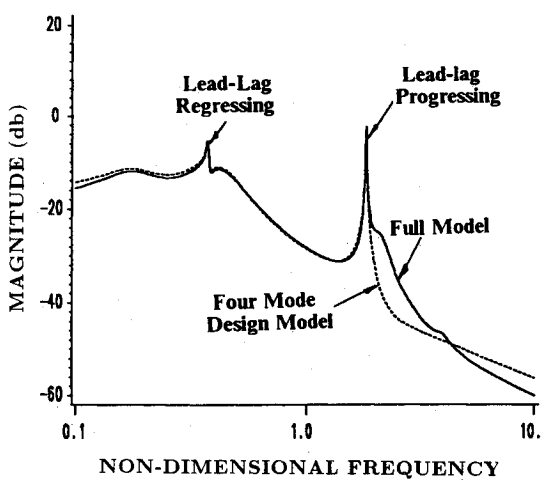

Fig. 5 Comparison of the singular values of the full model with the reduced model in hover at the nominal weight.

Table 2 Pole and zero data of full model in hover

Poles	$\dot{\theta}_x/\Delta\theta_{1s}$ zeros	$\dot{\theta}_x/\Delta\theta_{1c}$ zeros
$0.0006 \pm j0.0044$	$-0.3281 \pm j3.9563$	8.8707
$-0.0006 \pm j0.0044$	2.9792	$-0.5480 \pm j4.1587$
$-0.0523 \pm j0.1682$	$-0.3019 \pm j1.9800$	$-1.5028 \pm j3.4393$
$0.0044 \pm j0.3709$	$-0.1671 \pm j1.8729$	$-0.2607 \pm j1.9643$
$-0.0922 \pm j0.4011$	$-0.0858 \pm j0.8532$	$-0.1406 \pm j1.8178$
$-0.7024 \pm j0.0140$	$-0.7306 \pm j0.2014$	-0.7086
$-0.0063 \pm j1.8335$	-0.4912	-0.3627
$-0.2781 \pm j1.9641$	$-0.0133 \pm j0.3836$	$-0.0008 \pm j0.3726$
$-0.1928 \pm j2.1172$	-0.0234	$-0.0590 \pm j0.1956$
$-0.2816 \pm j3.9670$	$0.0011 \pm j0.0082$	$0.0000 \pm j0.0043$
	-0.0001	0.0001
	0.0000	0.0000

Table 3 Pole and zero data of eight-state reduced model in hover

Poles	
$-0.0523 \pm j0.1682$	Body pitch
$0.0044 \pm j0.3709$	Lead-lag regressing
$-0.0922 \pm j0.4011$	Body roll
$-0.0063 \pm j1.8335$	Lead-lag progressing
Zeros	
$\dot{\theta}_x/\Delta\theta_{1s}$	$\dot{\theta}_x/\Delta\theta_{1c}$
$-0.0075 \pm j0.9217$	$-0.1826 \pm j2.1166$
$-0.6576 \pm j0.0000$	$-0.0596 \pm j0.1906$
$-0.0135 \pm j0.3836$	$-0.0003 \pm j0.3726$
-0.0200	-0.9926
-13.2327	

Equation (6) guarantees stability, if the error in the model is precisely as described in Eq. (4).

The design process could be carried out using plots of the singular values of $T=GK(I+GK)^{-1}$ and $S=(I+GK)^{-1}$, where the parameters of the LQG problem are varied in order to adjust the size of each of these transfer-function matrices in the appropriate frequency range.[12] However, in this paper, the singular values of the open-loop feedforward cascade GK are used. This is based on the approximation that when $\bar{\sigma}[T(j)) \ll 1$, then $\bar{\sigma}[T(j\omega)] \simeq \bar{\sigma}[G(j\omega)K(j\omega)]$ and the maximum singular value of the open-loop transfer function GK must be less than the inverse of l_m for stability to be guaranteed. In order to achieve this desired result, a full-state design with an appropriate loop shape is designed and then loop transfer recovery (LTR) is used to recover this shape.[10]

To discuss the method as used in this paper, the input and state weight matrices are defined as

$$R = \rho_c^2 I \tag{7}$$

$$Q = q_c^2 HH^T + Q_0 \tag{8}$$

in the regulator and

$$E[w_0 w_0^T] = \rho_f^2 I \tag{9}$$

$$E[w_s w_s^T] = q_f^2 FF^T \tag{10}$$

in the filter problem. The first step in the method is the filter design, where ρ_f, q_f, and F are selected to give a filter gain K_f. These values are selected to give desired loop properties defined by the maximum and minimum singular values of the transfer-function matrix $C(sI-A)^{-1}K_f$. The guidelines for selecting this loop shape are those which were previously described for selecting the loop shape $G(s)K(s)$. Once the desired loop shape is determined, the second step is to recover it through the regulator by setting $H=C$ and letting q_c approach a large value. This second step is based on the result

$$G(s)K(s) \to C(sI-A)^{-1}K_f \qquad \text{as} \qquad q_c \to \infty \tag{11}$$

Table 4 Closed-loop poles using the eight-state controller

$-0.44447 \pm j2.0286$	
$-0.07985 \pm j1.8333$	Lead-lag progressing
$-0.30337 \pm j0.37971$	
$-0.03659 \pm j0.37472$	
$-0.00780 \pm j0.37441$	Lead-lag regressing
$-0.10205 \pm j0.17774$	
$-0.06748 \pm j0.17178$	
-1.0290	
-152.52	

for minimal phase $G(s)$; i.e., no transmission zeroes in the right half of the s plane. The requirement that $G(s)$ be minimal phase is necessary since the recovery process of Eq. (11) inverts the plant dynamics making zeroes of $G(s)$ the poles of the compensator $K(s)$. If the zeroes are in the right half of the s plane, then with a large enough gain the compensator poles eventually become unstable. The procedure previously discussed is sometimes referred to as "sensitivity recovery," and it should be noted that a dual-recovery procedure is possible and is referred to as "robustness recovery."

Controller Design

The design approach of this paper is to select an operating point to design a constant-gain controller, and use this controller throughout the operating range of the helicopter. The design point is chosen to be in hover ($\mu = 0$), with the nominal weight ($M_F = 32$), which is a point near the region of worst instability for the configuration.

A single roll-rate measurement of the fuselage and the sine and cosine swashplate inputs are chosen to control the instability. The selection of the inputs is based on the previous control studies, which demonstrated the ineffectiveness of the collective swashplate input in controlling the air resonance instability in forward flight.[8] The roll rate is selected as the measurement since it is with the fuselage roll mode that the lead-lag motion of the blades interacts during the air resonance instability. Examination of the eigenvectors of the unstable mode confirms this and shows that the roll motion is dominant when compared to the pitch motion. The lead-lag degrees of freedom of the blades also could serve as measurements, but it is preferable to use measurements taken from a nonrotating reference frame (i.e., the frame of the fuselage). This avoids the problem of transmitting signals across the rotor head, which is not impossible, but doing so does complicate the control-system implementation.

The full model with the given set of inputs and output is minimal phase, with only one transmission zero at zero. The full model poles and zeroes for each channel are shown in Table 2. The collective and differential rotor modes have been removed as well as all other unobservable and uncontrollable modes leaving a 20th-order model in hover. The linear description, in block-diagonal modal form, of the two-input/one-output model is given in the Appendix. The original loop transfer recovery (LTR) procedure discussed in Ref. 10 required square plants, and if the plant was not square a "squaring-up" procedure was required. However, recent work showed that LTR was valid for nonsquare minimum phase systems, which made the "squaring-up" of a nonsquare system unnecessary.[13]

In order to keep the compensator order low, a reduced model is formed and used in the block design process. This reduction is accomplished by transforming the full system to block diagonal modal form and then removing the modes from the full model that are deemed unnecessary to characterize the system dynamics in the frequency range of interest. The balanced realization method of Ref. 14 would be preferable, but this technique is applicable to stable systems, which is not the case for the model of this paper. An acceptable design model is one consisting of the body roll, body pitch, lead-lag regressing, and the lead-lag progressing modes. The open-loop poles and zeroes of the design model are given in Table 3 and the order of the modal states is the same as the order of the listed modes. The collective and differential lead-lag modes are near the frequency range of the air resonance instability (Fig. 3), but are not retained since they are uncontrollable and unobservable in the hover condition. The low-frequency body modes are also not retained in the model since control over these modes is not the objective of this paper. These modes are in the frequency range of order 0.01/rev, which is a full decade below the frequency range of interest. Therefore, it is assumed that a high-pass filter can be used if necessary to leave these modes unaffected by the air resonance controller. This would also prevent any interaction of the controller with pilot inputs or any stability augmentation system (SAS) on the vehicle for controlling the low-frequency body modes.[15]

The design model is eighth-order and closely resembles the full model, as can be seen in the singular-value plot shown in Fig. 5. The reduced model is very close to the full model in the frequency range of interest capturing the peak due to the lead-lag regressing mode, which is the unstable mode that is to be controlled. The model also captures the sharp peak of the other dominant mode of the system, which is the lead-lag progressing mode. Naturally, removal of the higher- and lower-frequency modes produces the errors in these regions. The gain and phase plots for each input/output combination were also compared for the full and reduced models and they too showed good agreement up to a frequency near 1/rev.

A reduced model is being used in the design and care must be exercised in the placement of the crossover so there is sufficient rolloff to account for model error. The reduced model is valid in the frequency range below 1/rev, so the crossover of the loop shape should not greatly exceed this value. This is not overly restrictive since the loop crossover would have to be placed below 1/rev for other reasons. The rotor model is not

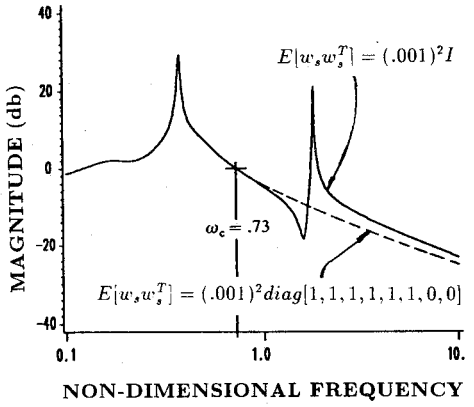

Fig. 6 Loop shapes of GK.

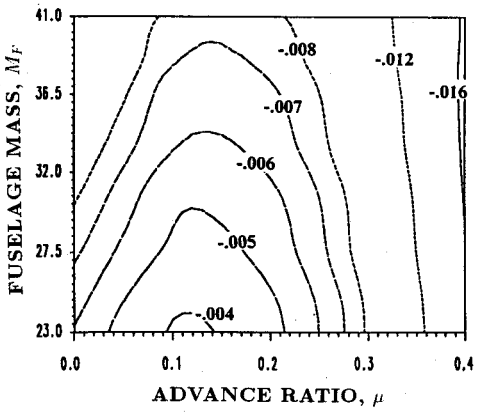

Fig. 7 Closed-loop nondimensional real part of the eigenvalue associated with the lead-lag regressing mode.

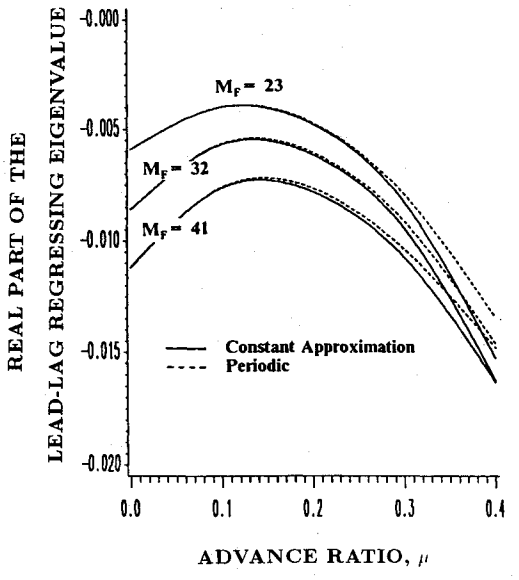

Fig. 8 Closed-loop nondimensional real part of the eigenvalue associated with the lead-lag regressing mode using the periodic and constant models.

expected to be highly accurate very much above the 1/rev frequency. Higher-order flexible modes and far better aerodynamic models would be necessary for the mathematical model to be valid much beyond this frequency. In addition, all helicopters have an unavoidable 1/rev noise, which arises from differences in each of the individual blade forces around the rotor (e.g., variations in blade mass produce differences in inertial forces). This effect is difficult to model accurately and is not included in the model of this paper, but its effect must be considered as an error that could interfere with the control task. Thus, the crossover frequency of the air resonance controller should be restricted below the 1/rev frequency.

With the design model chosen, the next step might be to generate the error function by generating models at various operating points. However, this approach is of dubious value. In theory, once l_m is defined the closed-loop stability can be checked through Eq. (6) without rechecking the stability at the full range of operating conditions. Unfortunately, as stated before, Eq. (6) is only true if the errors in the system are precisely as indicated in Eq. (4) (i.e., a multiplicative unstructured uncertainty at the model output), which is not necessarily the case. Because of this, a check of the closed-loop stability using the controller on the full model throughout the operating range is still necessary. In addition, the performance of the controller is determined by the amount of damping in the lead-lag regressing mode, which also requires that the design be checked at all of the operating points. For these reasons, the design is simply based on known properties of helicopter dynamics and the known limitations in the mathematical model, as previously discussed, as well as the known error between the reduced model and the full model. Stability and performance of the controller is then checked directly at all of the off-design operating points.

Initially, a controller was designed by choosing the filter noise covariances as $E[w_s w_s^T] = (0.001)^2 I$ and $E[w_o w_o^T] = (0.001)^2$. This choice gave a loop shape as shown in Fig. 6, which was recovered using $R = I$ and $Q = 0.3^2 I + q_c^2 C^T C$ with $q_c = 10{,}000$. This loop shape has a peak near the progressing lead-lag mode far in excess of the allowable error for guaranteed stability. The difference between the full and reduced model as seen in Fig. 5 indicates that GK should be approximately -15 dB near the 1.8/rev frequency. Application of this controller on the full model yielded a stable lead-lag regressing mode and progressing mode. The flap progressing mode was strongly destabilized throughout most of the operating range of the vehicle. This mode was only marginally stable at a very high loading condition, and below $M_F = 37$ the mode is unstable for all advance ratios.

This problem was removed by adjusting the state-noise covariance to $E[w_s w_s^T] = (0.001)^2$ diag[1,1,1,1,1,1,0,0], which gives the loop shape indicated in Fig. 6. This choice gives input noises into all modes except the lead-lag progressing mode and effectively filters this mode out of the loop shape. The loop shape of this controller has only one crossover frequency near 0.73. The peak near 1.8 is eliminated, and the only region of high gain is near the instability. Overall, this loop shape fits into the acceptable criteria as previously mentioned. The closed-loop poles of this controller are presented in Table 4. The application of this controller on the full model throughout the operating conditions gives a stable lead-lag regressing mode as shown in Fig. 7. The nondimensional real part of the lead-lag regressing eigenvalue is stable throughout the flight regime being the weakest in the vicinity of $M_F = 23$ and $\mu = 0.11$. All other modes remain stable.

A check of the controller is made to verify that the periodic terms in the full model do not significantly alter the stability results. Figure 8 shows a comparison of the real part of the lead-lag regressing eigenvalue at three weight conditions for the constant-coefficient approximation and the full periodic model. A very small weakening of the stability occurs at an advance ratio of 0.4 for the three loading conditions. These comparisons support the use of a constant-coefficient design model, although the adverse shift in the regressing mode suggests that a final check with the periodic terms of the model is necessary. Time simulations using the linear model showed that excessively large control inputs are not necessary to suppress the air resonance instability. A time simulation showed that the closed-loop system could suppress angular roll rates as large as 6.5 deg/s with <2 deg of swashplate input.

Attempts were made to further reduce the order of the controller by using a six-state design model. Since the lead-lag progressing mode is outside of the desired bandwidth of the $G(s)K(s)$ transfer function matrix, this mode was removed. The filter matrices were chosen as before with $E[w, w_s^T] = (0.001)^2 I$ and $E[w_o w_o^T] = (0.001)^2$, where the identity matrix is now 6×6. The regulator matrices were kept the same. The loop shape that resulted is the same as the single peaked shape shown in Fig. 6. Although the loops are identical for the controller designed with the lead-lag progressing mode and the controller design without this mode, the reader is reminded that the two controllers are not the same. The error model between the full model and the six-state model would be significantly larger at the 1.8/rev frequency and the loop shape would violate the stability sufficiency condition. A check of the closed-loop poles using the six-state controller resulted in an unstable lead-lag progressing mode throughout the operating condition of the helicopter. It is true that the progressing mode is outside the bandwidth of the loop $G(s)K(s)$, but its proximity to the lead-lag regressing mode and its intensity are such that the system rolloff that results from the LTR method is inadequate to compensate for the error that results from neglecting this mode.

Conclusions

A coupled rotor/fuselage helicopter model with the effects of blade torsional flexibility, unsteady aerodynamics, and forward flight was used to demonstrate the use active control to stabilize air resonance. The controller was shown to stabilize the system throughout a range of loading conditions between $\pm 30\%$ of the nominal weight, and a range of forward flight speeds between $\mu = 0$ to 0.4. The controller uses a single roll-rate measurement, which is in the frame of the fuselage, avoiding the need to send signals across the rotor head, and uses the sine and cosine inputs allowing the use of a conventional swashplate mechanism. The controller was synthesized using the LQG/LTR multivariable frequency-domain technique and was based on a design model composed of the body

Table A1 Open-loop system in block-diagonal modal form

$A(2\times2)$ Blocks		B $\Delta\theta_{1s}$	$\Delta\theta_{1c}$	C^T $\dot{\theta}_x$
0.0006	0.0044	2.6816	−1.7454	0.0001
−0.0044	0.0006	−1.7129	−2.6821	0.0000
−0.0006	0.0044	2.1639	2.5878	−0.0001
−0.0044	−0.0006	−2.4577	2.0810	0.0001
−0.0523	0.1682	0.0807	0.0238	0.1832
−0.1682	−0.0523	−0.0663	0.0302	−0.0503
0.0044	0.3709	0.0266	0.0221	0.0014
−0.3709	0.0044	0.0360	−0.0086	−0.1107
−0.0922	0.4011	−0.0516	−0.0900	0.1470
−0.4011	−0.0922	−0.0221	0.1465	0.2160
−0.7024	0.0140	−0.1714	−0.0775	0.0379
−0.0140	−0.7024	0.1369	−0.2894	0.0464
−0.0063	1.8335	−0.0362	−0.0166	0.0708
−1.8335	−0.0063	0.0107	−0.0322	0.1819
−0.2781	1.9641	0.0873	0.0486	0.0091
−1.9641	−0.2781	0.0534	−0.0727	−0.0060
−0.1928	2.1172	0.5054	0.1207	−0.0197
−2.1172	−0.1928	−0.1209	0.5035	0.0027
−0.2816	3.9670	−0.2133	−0.1684	−0.0001
−3.9670	−0.2816	0.1665	−0.2230	−0.0013

roll and pitch modes and the lead-lag regressing and progressing modes.

Appendix: Linear Model in Hover

The linear model used to design the controller is given in Table A1 in block-diagonal modal form. The first two columns are the 2×2 blocks that are along the diagonal of the A matrix. The diagonal elements of each of the 2×2 blocks are the real part of the eigenvalue associated with a particular mode of the system, while the off-diagonal elements are the $\pm$ imaginary parts of the eigenvalue. The corresponding elements in the B matrix and the C matrix are given in the subsequent columns. The inputs of the system are the sine input $\Delta\theta_{1s}$ and the cosine input $\Delta\theta_{1c}$, while the output is the roll rate $\dot{\theta}_x$.

Acknowledgment

This research was funded by NASA Ames Research Center, Moffett Field, CA, under Grants NAG 2-209 and NAG-477.

References

[1]Burkam, J. E., and Miao, W., "Exploration of Aeroelastic Stability Boundaries with a Soft Inplane Hingeless Rotor Model," *Journal of the American Helicopter Society,* Vol. 17, No. 4, 1972, pp. 27–35.

[2]Donham, R. E., Cardinale, S. V., and Sachs, I. B., "Ground and Air Resonance Characteristics of a Soft Inplane Rigid Rotor System," *Journal of the American Helicopter Society,* Vol. 14, No. 4, 1969, pp. 33–44.

[3]Straub, F. K., and Warmbrodt, W., "The Use of Active Controls to Augment Rotor/Fuselage Stability," *Journal of the American Helicopter Society,* Vol. 30, No. 3, July 1985, pp. 13–22.

[4]Straub, F. K., "Optimal Control of Helicopter Aeromechanical Stability," *Vertica,* Vol. 11, No. 3, 1987, pp. 12–22.

[5]Young, M. I., Bailey, D. J., and Hirschbein, M. S., "Open- and Closed-Loop Stability of Hingeless Rotor Helicopter Air and Ground Resonance," Paper 20, NASA SP 352, 1974.

[6]Takahashi, M. D., "Active Control of Helicopter Aeromechanical and Aeroelastic Instabilities," Ph.D. Dissertation, Univ. of California, Los Angeles, Los Angeles, CA, June 1988.

[7]Pitt, D. M., and Peters, D. A., "Theoretical Predictions of Dynamic Inflow Derivatives," *Vertica,* Vol. 5, No. 1, 1981, pp. 21–34.

[8]Takahashi, M. D., and Friedmann, P. P., "Active Control of Helicopter Air Resonance in Hover and Forward Flight," AIAA Paper 88-2407, *Proceedings of the AIAA/ASME/ASCE/AMS/ACS 29th Structures, Structural Dynamics, and Materials Conference,* Vol. 3, AIAA, Washington, DC, 1988, pp. 1521–1532.

[9]Horowitz, I. M., and Shaked, U., "Superiority of Transfer Function Over State-Variable Methods in Linear Time-Invariant Feedback System Design," *IEEE Transactions on Automatic Control,* Vol. AC-20, No. 1, 1975, pp. 84–97.

[10]Doyle, J. C., and Stein, G., "Multivariable Feedback Design: Concepts for a Classical/Modern Synthesis," *IEEE Transactions on Automatic Control,* Vol. AC-26, No. 1, 1981, pp. 4–16.

[11]Stein, G., "The LQG/LTR Procedure for Multivariable Feedback Control Design," *IEEE Transactions on Automatic Control,* Vol. AC-32, No. 2, 1987, pp. 105–114.

[12]Safonov, M. G., Laub, A. J., and Hartmann, G. L., "Feedback Properties of Multivariable Systems: The Role and Use of the Return Difference Matrix," *IEEE Transactions on Automatic Control,* Vol. AC-26, No. 1, 1981, pp. 47–65.

[13]Madiwale, A., and Williams, D. E., "Some Extensions of Loop Transfer Recovery," *Proceedings of the American Control Conference,* Vol. 2, 1985, pp. 790–795.

[14]Moore, B. C., "Principal Component Analysis in Linear Systems —Controllability, Observability, and Model Reduction," *IEEE Transactions on Automatic Control,* Vol. AC-26, 1981, pp. 17–32.

[15]Johnson, W., *Helicopter Theory,* Princeton University Press, Princeton, NJ, 1980, Chap. 15.